Investigation of the performance and thermal decomposition of MgO and MgO-SiO_2 formulations

C. Sonat[a], C. Unluer[a,*]

[a] School of Civil and Environmental Engineering, Nanyang Technological University, 50 Nanyang Avenue, Singapore 639798, Singapore

* Corresponding author. Tel.: +65 91964970, E-mail address: ucise@ntu.edu.sg

Abstract

The use of magnesium oxide (MgO) as the key reactive component within hydraulic binder systems has been reported in many studies. This study investigated the strength and microstructural development of MgO and MgO-SiO_2 binder systems under different curing conditions. Concrete samples, whose binder component consisted of only MgO or MgO-SiO_2 were subjected to ambient and carbonation curing conditions for 56 days. The compressive strength results were supported with microstructural analysis performed via XRD, TG/DTG and FESEM. While the formation of brucite within MgO samples led to limited strength under ambient conditions, MgO-SiO_2 samples demonstrated a steady strength development due to the formation of M-S-H. Incorporation of carbonation curing enhanced the mechanical performance of both systems, enabling rapid strength development that reached up to 77 MPa at 7 days. This increase in strength was associated with the densification of microstructure via the formation of Mg-carbonates, which were assessed via thermal analysis.

Keywords: MgO; Hydration; Carbonation; Compressive strength; Microstructure; Thermal decomposition

1 Introduction

The high energy consumption and CO_2 emissions associated with Portland cement (PC) production [1] have driven the need for alternative building materials. Reactive magnesium oxide (MgO)-based cementitious materials are a group of materials that have lower calcination temperatures than PC (i.e. 700 vs. 1450 °C) and ability to gain strength via various routes, some of which involve the sequestration of CO_2 in the form of stable carbonates [2, 3] or the formation of magnesium silicate hydrate (M-S-H) within MgO-SiO_2-H_2O systems [4-6].

Recent research on MgO-SiO_2-H_2O systems have shown that the formation of M-S-H via a reaction between a Mg-based source (e.g. MgO, $Mg(OH)_2$) and a silica source (e.g. microsilica) results in a binder that can be used in certain applications such as waste encapsulation [7-9], refractory castables [10] and building materials [4]. The mix designs introduced in these studies usually involve the use of a dispersant, sodium hexametaphosphate ($(NaPO_3)_6$, SHMP), to reduce the water demand and improve the rheological properties of the fresh mix. The reduction of water content through the use of SHMP in MgO-silica fume mixes was reported to enable 28-day strengths as high as 70 MPa [4].

Within MgO-SiO_2 formulations, the formation of M-S-H can take place via the reaction between Mg^{2+} and dissolved silica complexes [5, 11]. The main factors influencing M-S-H formation are the chemical and physical properties of the precursors, mix composition, curing conditions and pH of the pore solution. A recent study has shown that M-S-H can form directly from the reaction of MgO with SiO_2 or from the consumption of the previously formed $Mg(OH)_2$ (brucite), depending on the SHMP content within the initial mix design [12]. The formation of M-S-H ceases when either the magnesia or silica source is fully consumed in the reaction [13]. Therefore, within mixes containing relatively high initial MgO contents, M-S-H can be accompanied with unreacted MgO and the hydrate phase of MgO, $Mg(OH)_2$. Previous studies [14] reported the presence of brucite in reactive MgO-SiO_2 samples even after 90 days of curing.

Differing from $MgO\text{-}SiO_2\text{-}H_2O$ systems, carbonated MgO systems rely on the formation of hydrated magnesium carbonates (HMCs) for strength gain. This usually initiates with the hydration reaction of MgO into brucite, followed by the carbonation reaction to form a range of HMCs, as shown in Equations 1-5. The extent of the carbonation reaction, along with the morphology of these carbonate phases control the mechanical performance of carbonated MgO systems. Strength development of these binders is associated with the increase in sample density as carbonation is an expansive process that reduces the overall pore volume (i.e. the formation of HMCs causes a significant expansion and increases the solid volume by a factor of 1.8-3.1) and evolution of microstructure as the morphology and binding strength of the carbonate crystals contribute to the network structure.

$$MgO + H_2O \rightarrow Mg(OH)_2 \text{ (Brucite)} \quad (1)$$

$$Mg(OH)_2 + CO_2 + 2H_2O \rightarrow MgCO_3 \cdot 3H_2O \text{ (Nesquehonite)} \quad (2)$$

$$2Mg(OH)_2 + CO_2 + 2H_2O \rightarrow Mg_2CO_3(OH)_2 \cdot 3H_2O \text{ (Artinite)} \quad (3)$$

$$5Mg(OH)_2 + 4CO_2 \rightarrow Mg_5(CO_3)_4(OH)_2 \cdot 4H_2O \text{ (Hydromagnesite)} \quad (4)$$

$$5Mg(OH)_2 + 4CO_2 + H_2O \rightarrow Mg_5(CO_3)_4(OH)_2 \cdot 5H_2O \text{ (Dypingite)} \quad (5)$$

As carbonation is the main mechanism for strength gain within these systems, the diffusion of CO_2 into the sample matrix plays a key role in the final performance. This necessitates the provision of the necessary porosity to enable CO_2 ingress, which can be achieved via a carefully planned mix design. Studies focusing on carbonated systems have generally proposed the use of 4-40% MgO as the main binder, accompanied with fine and/or coarse aggregates, along with fly ash or slag in some formulations [15-21]. Although higher cement contents generally lead to higher strengths, this is associated with increased cost and environmental impacts. Therefore, achieving a balance amongst the mechanical, economical and sustainability aspects of the proposed mix designs is important. Independent of the cement content, these studies have shown that subjecting MgO samples to natural atmospheric exposure conditions containing ambient CO_2 levels (0.04%) are not

sufficient for the carbonation reaction to take place and provide high strengths even after several months [20, 22], therefore highlighting the need for accelerated carbonation conditions involving the use of elevated CO_2 concentrations (i.e. 5-20% in most cases). The use of these accelerated CO_2 concentrations was shown to enable compressive strengths as high as ~60 MPa after curing MgO-based concrete samples under 10% CO_2 for 28 days [15].

While the use of elevated CO_2 concentrations increases the rate and degree of carbonation to some extent, the presence of uncarbonated brucite is a common occurrence in carbonated MgO systems as the penetration depth of CO_2 is limited towards the sample core [16]. One of the main reasons for this is the precipitation of carbonation products on the outer surface, which prevents further carbonation of $Mg(OH)_2$, thereby limiting carbonation and associated strength development, and resulting in an inefficient use of MgO as a binder. Since uncarbonated brucite does not significantly contribute to strength development by itself due to its poor binding capacity, the conversion of brucite or unhydrated MgO into strength providing phases such as HMCs or M-S-H can be enabled via the development of a combined system involving the presence of M-S-H as well as a carbonate network.

Although the reaction mechanisms, properties and performance of both MgO-SiO_2-H_2O and carbonated MgO systems have been individually investigated to some extent, there are not any studies focusing on the combination of these two systems in the form of a multi-component binder. Since both systems rely on the dissolution of MgO and the subsequent hydration reaction as the initial step in their strength development, the use of carbonation to enhance the performance of this combined binder system is yet to be explored. This study aims to investigate the properties of binders involving the combination of MgO-SiO_2-H_2O and carbonated MgO systems and their capacity to increase the utilization of MgO and $Mg(OH)_2$ via the formation of an extensive network composed of Mg-carbonates and M-S-H. The influence of carbonation on the MgO-SiO_2-H_2O system was evaluated via a detailed comparison of MgO-SiO_2 and MgO-based concrete samples with the same binder content. The prepared samples were subjected to sealed and carbonation conditions to assess their performance with and without the introduction of CO_2 curing. The mechanical performance of the MgO-SiO_2 (MS) and MgO (M) systems was studied with

compressive strength testing at different durations up to 56 days. The strength results of each system were supported with an analysis of their microstructural development along different stages of curing. The formation of hydrate and carbonate phases were investigated via X-ray diffraction (XRD) and thermogravimetric/derivative thermogravimetric analysis (TG/DTG), while the microstructural development of the prepared formulations was observed by field emission scanning electron microscopy (FESEM).

2 Materials and Methodology

2.1 Materials

Reactive MgO (commercial name “calcined magnesite 92/200”) and microsilica (commercial name “940U”) were obtained from Richard Baker Harrison (UK) and Elkem Materials (Singapore), respectively. The properties of MgO and microsilica are listed in Table 1. SHMP, used as a superplasticizer, was obtained from VWR (Singapore). Saturated surface dry (SSD) gravel provided by Buildmate (Singapore) with a particle size of 4.7–9.5 mm and a density of 2.61 kg/m^3 was used to form the aggregate profile in the concrete samples prepared.

2.2 Mix composition and curing conditions

Table 2 shows the mix compositions prepared under this study and the corresponding curing conditions each mix was subjected to. Two different binder systems composed of MgO (M) and MgO-SiO_2 (MS), in which MgO and microsilica were introduced at a ratio of 1:1, were prepared. These binders were used in the preparation of concrete samples that were composed of 40% binder (i.e. to provide binding in the absence of fine aggregates, which were omitted from the mix design to avoid contamination with quartz and provide an accurate quantification of hydrate and carbonate phases during microstructural analysis) and 60% coarse aggregates, by mass. All formulations were prepared with a constant water/binder (w/b) ratio of 0.45 and included 1% (i.e. of the total binder content) of SHMP to improve fluidity,

which led to fully compacted samples for both systems. The prepared samples were subjected to two different curing conditions: (i) Sealed (S) under 95% relative humidity (RH), ambient temperature and ambient CO_2 concentration; and (ii) carbonated (C) under 95% RH, ambient temperature and 10% CO_2 concentration.

2.3 Sample preparation

Sample preparation started via the addition of SHMP into a predetermined amount of water, followed by its mixing for about 20 minutes to ensure it was fully dissolved. MgO was then slowly added into the water while mixing. For the preparation of MS samples only, microsilica was also gradually added into the mixing bowl during mixing. The mixing procedure continued for 10 minutes after all the powders were added to prepare a truly homogenized and thoroughly mixed paste, after which the coarse aggregates were introduced into the mix. The prepared concrete mix was poured into 50x50x50 mm cubic molds, which were consolidated by a vibrating table for 5 minutes and trowel finished to achieve full compaction. The prepared samples were kept under sealed conditions for 24 hours until demolding and were then placed into corresponding curing conditions. The masses of all samples were recorded before and after each curing duration to assess the changes in their densities under different conditions.

2.4 Methodology

2.4.1 Compressive strength

The compressive strength of the prepared concrete samples was measured by uni-axial loading in triplicates at 3, 7, 28 and 56 days. The equipment used for this purpose was a Toni Technik Baustoffprüfsysteme machine, operated at a loading rate of 55 kN/min.

2.4.2 XRD, TG/DTG and FESEM analyses

Samples extracted from the cubes crushed during compressive strength testing were stored in acetone for at least 3 days to stop hydration, followed by vacuum drying for another 7 days in preparation for XRD, TG/DTG and FESEM analyses. The vacuum dried samples were ground down to pass through a 75 μm sieve in preparation for XRD and TG/DTG.

XRD data was collected via a Bruker D8 advance instrument using Cu K_α radiation (40 kV, 30 mA) with a scanning rate of 0.02° 2θ/step from 10 to 80° 2θ. TG/DTG was conducted on a Perkin Elmer TGA 4000 equipment from 30 to 900 °C with a heating rate of 10 °C/min under nitrogen flow. The quantification of the formed phases within each sample was performed via the deconvolution of the DTG curves and the calculation of the area corresponding to different decomposition reactions under each deconvoluted curve. For the observation of the sample microstructures via FESEM analysis, the vacuum dried samples were coated with platinum. The morphologies of the hydration and carbonation products within the prepared samples were investigated via FESEM images obtained by a JEOL JSM-7600F equipment.

3 Results and Discussion

3.1 Density

The wet density values of all samples over the 56 days of curing are shown in Figure 1. The initial densities of M samples before the start of the curing process were ~8% higher than those of MS samples (2.33 vs. 2.16 g/cm^3). This was associated with the differences in the compositions of the binder components of each system. For both systems, samples cured under sealed conditions (M-S and MS-S) revealed relatively constant densities throughout the curing process. Any increase in density due to the progress of the hydration reaction that resulted in the expansive formation of hydrate phases within these samples could have been partially overshadowed with the loss of unbound water from the pore system during curing. Alternatively, the introduction of carbonation led to a noticeable increase in the densities of both systems. The

densification process was more visible within M-C samples, which demonstrated ~5% increase in their densities over 56 days, revealing a final density of 2.44 g/cm^3. Corresponding MS-C samples revealed an increase of ~1.5% over 56 days. The final density of MS-C samples was recorded as 2.19 g/cm^3, which was lower than that of M samples, similar to the trend observed before curing initiated. Apart from the initial and final densities, the change in the sample density over time during the curing process could be an indication of the performance of each formulation under different curing conditions.

3.2 Compressive strength

Compressive strengths of samples cured for up to 56 days are shown in Figure 2. Carbonated MgO (M-C) samples achieved the highest strengths amongst all samples throughout the entire curing duration. The corresponding MgO samples that were subjected to sealed conditions (M-S) revealed the lowest strengths of around 18 MPa, which remained relatively stable throughout 56 days due to the low ambient CO_2 concentrations that slowed down the carbonation process. Alternatively, the rapid strength gain exhibited by M-C samples was associated with the elevation of the CO_2 concentration to 10% during the curing process, which was in line with the findings of previous studies [20, 23]. The presence of CO_2 enabled the carbonation reaction within M-C samples, which reached early-age strengths as high as 56 and 77 MPa at 3 and 7 days, respectively. The difference in the CO_2 concentration used in the curing of M-S and M-C samples led to an up to ~330% difference in their performance. This significant transformation in strength is a clear indication of the critical role that carbonation plays in the mechanical performance of MgO-based formulations, whose strength gain dominantly relies on the formation of carbonate phases, as reported in the literature [3, 17, 20, 24]. This increase in strength within the carbonated samples was in line with the increase in the density of samples reported earlier in Figure 1, where M-C samples revealed a noticeable increase in their density due to the formation of carbonates.

Samples, whose binder component consisted of MgO-SiO_2 (MS-S and MS-C), demonstrated a consistent strength development over 56 days. The use of

carbonation curing in MS-C samples enabled 56-day strengths as high as 73 MPa, while the corresponding MS-S samples cured under sealed conditions revealed a strength of 56 MPa. The difference in strength was more pronounced at early ages (3 days), during which MS-C samples achieved up to ~60% higher strengths than MS-S samples. This difference gradually reduced and stabilized at ~20% for the remaining curing durations. The high difference at earlier ages was mainly due to the different curing conditions these two sets of samples were subjected to. While the formation of M-S-H was the main source of strength in MS-S samples, the higher strengths obtained by MS-C samples were attributed to the formation of carbonate phases. As the carbonation process takes place more rapidly at early stages of curing and gradually slows down with the densification of the microstructure, the trends observed in the strength difference of MS-S and MS-C samples were in line with the expected progress of carbonation.

Amongst the four sets of samples prepared under this study, those subjected to carbonation curing (M-C and MS-C) demonstrated the best performance for each binder composition (MgO and MgO-SiO_2). Although the highest strengths were achieved by M-C samples at early ages (≤ 7 days), the consistent strength development of MS-C samples led to similar results at longer durations (≥ 28 days). In addition to the binding strength associated with the carbonate network that formed during the curing process, the higher densities revealed by M-C samples in comparison to MS-C samples may have contributed to their strength development. Alternatively, while the formation of M-S-H within MS-S samples resulted in a considerable performance without carbonation, the incorporation of carbonation in the curing process significantly enhanced the strength development of these samples. However, when compared to MgO-SiO_2 (MS) samples, which also gained strength via the hydration process that led to the formation of M-S-H; the progress of carbonation was much more critical for purely MgO-based (M) samples, whose strength development mainly depended on the conversion of Mg-phases (MgO and $Mg(OH)_2$) into carbonates.

3.3 Microstructure

Figure 3 shows the FESEM images of all samples after 3 days of curing. M-S sample (Figure 3 (a)) indicated a loose formation of brucite around MgO particles, whereas an extensive formation of various HMCs, namely needle-like nesquehonite and rosette-like hydromagnesite/dypingite, were observed in the M-C sample (Figure 3 (b)). The dense formation of these HMCs could explain the high strength gain (56 MPa) achieved by M-C samples at as early as 3 days. Similar to M-S, MS-S sample (Figure 3 (c)) mainly displayed the formation of brucite (i.e. lamellar aggregates of platelets [25]) along with M-S-H (i.e. continuous layer covering other particles [14, 26]), which slightly led to the densification of the microstructure. The resemblance in the microstructures of M-S and MS-S samples corresponded well with their identical 3-day strengths. The use of carbonation curing in MS-C sample (Figure 3 (d)) clearly revealed the formation of rosette-like hydromagnesite/dypingite with large flakes, along with M-S-H, which could explain the higher strengths obtained by this sample in comparison to MS-S. The morphology of hydromagnesite/dypingite observed within MS-C sample differed from those seen in M-C, where the agglomeration of smaller crystals produced a denser microstructure. Coupled with the dense formation of nesquehonite needles, the densification of the sample microstructure can explain the carbonation-related rapid strength gain of M-C at 3 days.

Figure 4 shows the FESEM images of all samples after 28 days of curing. Although it was cured for a longer duration, M-S sample (Figure 4 (a)) mainly indicated the formation of brucite along with unreacted MgO. The limited formation of carbonates was as expected since the ambient concentration of CO_2 used during the curing of M-S samples was not sufficient for a noticeable formation of carbonates, thereby limiting strength development. Differing from M-S, M-C sample (Figure 4 (b)) revealed the dense formation of interlocked nesquehonite and artinite, along with hydromagnesite/dypingite. The simultaneous formation of various carbonate phases corresponded well with the highest strengths obtained by M-C samples, which outperformed all others during the entire curing period. Formation of a continuous gel-like M-S-H layer, similar to those reported in earlier studies [14, 26], was observed in the microstructure of MS-S sample (Figure 4 (c)), which could explain its steady strength development with time. The spherical SiO_2 particles were less abundant when compared to the microstructure of MS-S sample cured for 3 days. The reduction in the amount of SiO_2 was in line with the increase in M-S-H formation

as silica was consumed in the hydration reaction over time. When subjected to carbonation, MS-C sample (Figure 4 (d)) exhibited the presence of a dense nesquehonite cluster, which formed a wall-like structure via the combination of individual needles. Along with nesquehonite, rosette-like hydromagnesite/dypingite agglomerates contributed to the densification of the microstructure. Amongst the HMCs, the loose presence of spherical SiO_2 particles was observed, whereas the gel-like M-S-H largely disappeared from the microstructure. The lack of M-S-H, accompanied with the abundant presence of SiO_2 particles, where MS-C sample differed from the corresponding MS-S sample that was cured under ambient conditions, could be an indication of the conversion of Mg-based initial phases to Mg-carbonates under the presence of CO_2 curing.

3.4 XRD

The XRD diffractograms of all samples cured for 3 days are shown in Figure 5. The brucite peaks were accompanied with unreacted MgO (periclase) peaks in all samples, whose presence was an indication of the limited progress of hydration during the first 3 days of curing. The M samples, whose binder component was composed of MgO only, demonstrated brucite peaks with noticeably higher intensities than those of MS ($MgO\text{-}SiO_2$) samples. This difference in the brucite peaks could be attributed to the higher initial MgO content of the M samples when compared to MS samples (40 vs. 20 wt% of the total mix composition) and the potentially higher consumption degree of the brucite that may have initially formed within the MS system, via its reaction with the dissolved silica to form M-S-H and carbonation (in the MS-C sample).

Apart from MgO and brucite, the presence of small amounts of silica and magnesite (the latter from the incomplete decomposition of the parent material during the production of MgO) was observed as impurities in all samples. While the XRD patterns of MS-S and MS-C were similar, a small presence of hydromagnesite/dypingite was observed in MS-C samples, which was in line with the microstructural observations reported earlier in Section 3.3. These were accompanied with unreacted amorphous silica peaks centered around 21° 2θ. The

slight formation of amorphous M-S-H was observed at around 35° and 60° 2θ [4, 7] in both MS samples, albeit more visibly within the MS-S sample. This difference was associated with the variations in the environments used for the curing of these samples, during which MS-C was subjected to carbonation. The use of carbonation curing limited the formation of M-S-H and resulted in the slight presence of carbonates instead, similar to M-C samples. Although the formation of carbonate phases within M-C and MS-C samples was clearly observed in their microstructures reported in Section 3.3, these phases did not reveal high intensities in the XRD patterns obtained at 3 days. This could be due to the relatively lower intensities of these phases in comparison to major phases such as MgO and brucite and the variations in the carbonation degree, which reduced with sample depth. These results can be an indication that although the progress of carbonation was limited in M-C and MS-C samples, it still significantly enhanced the mechanical performance of these samples in comparison to the corresponding uncarbonated samples at as early as 3 days.

Figure 6 shows the XRD diffractograms of all samples cured for 28 days. Although the presence of MgO could still be observed in all samples, a reduction in its intensity was anticipated in comparison to those observed at 3 days to demonstrate the progress of hydration and carbonation between these periods. While the brucite peaks were present in all samples, they were less prominent within samples subjected to carbonation for each composition. The brucite peaks were accompanied with various HMCs such as hydromagnesite, dypingite, artinite and nesquehonite within M-C samples, which corresponded well with microstructural observations. Alternatively, the amorphous bands of M-S-H located at around 25°, 35° and 60° 2θ [13] were clearly revealed in the XRD pattern of MS-S samples. In addition to M-S-H, small peaks of MgO and brucite were also present within MS-S, indicating that there was still room for improvement for the complete utilization of MgO. Subjecting the same composition to carbonation led to the disappearance of brucite and the reduction in the amount of residual MgO in MS-C samples. The simultaneous appearance of various HMCs was a clear demonstration of the carbonation reaction within the $MgO\text{-}SiO_2$ system. The lack of M-S-H peaks, accompanied with the presence of unreacted silica at around 21° 2θ within MS-C samples indicated the conversion of Mg-phases into carbonates under carbonation curing, which confirmed

the microstructural observations (Section 3.3) and strength results (Section 3.2) reported earlier.

3.5 TG/DTG

Figure 7 shows the TG and DTG plots of all samples cured for 28 days. Since all samples were subjected to vacuum drying before testing, the total mass loss observed during this process mainly corresponded to the decomposition of hydrate and carbonate phases. When the total mass loss values revealed by each sample were compared, it could be seen that MS-S sample revealed lower values than others. This difference could be partially attributed to the higher initial MgO contents of M samples in comparison to MS samples, which could have led to the formation of a larger amount of hydrate and/or carbonate phases. Furthermore, the formation of carbonate phases within sample MS-C led to a higher mass loss than those of MS-S. Regardless of the initial composition, amongst each binder composition (MgO and MgO-SiO_2), those subjected to carbonation led to higher mass losses due to the decomposition of HMCs. In carbonated MgO systems, the dehydration, dehydroxylation and decarbonation of common HMCs (e.g. nesquehonite, artinite, hydromagnesite and dypingite) were reported to take place at < 250, 250-500, and > 350 °C, respectively [27-30]. In MgO-SiO_2-H_2O systems, the main steps involved during the thermal decomposition of M-S-H and other phases can be summarized as below [31, 32]:

1. 30-300 °C: Loss of interlayer water of M-S-H

2. 300-750 °C: Decomposition of uncarbonated brucite and separation of hydroxyl groups in M-S-H

3. 750-900 °C: Dehydroxylation of silanol groups

Amongst the samples cured under sealed conditions, the much lower mass loss of MS-S than that of M-S was accompanied with its higher strengths than sample M-S. This difference in the strengths of these two uncarbonated samples could be linked

with the variations in the hydrate phases that formed within the MgO (brucite) and MgO-SiO_2 (M-S-H with a minor formation of brucite) formulations. This variation was also demonstrated by the DTG plots in Figure 7(b), where the two peaks at 95 and 405 °C within MS-S sample referred to the loss of interlayer water and separation of hydroxyl groups of M-S-H along with the decomposition of a small amount of brucite, respectively. Alternatively, the thermal decomposition of M-S sample revealed a large endothermic peak at ~425 °C corresponding to the decomposition of brucite, which was in line with the XRD patterns shown in Figure 6. When the 28-day strength results of these two samples were compared, the larger contribution of M-S-H to the strength development of MS-S sample than that of brucite, whose extensive formation was clearly observed in M-S sample, could be confirmed.

The introduction of carbonation at a CO_2 concentration of 10% during the curing of M-C and MS-C samples led to the appearance of additional peaks associated with the formation of carbonate phases. The DTG plots of these samples revealed two additional endothermic peaks centered at around 224-263 and 491-507 °C, corresponding to the dehydroxylation and decarbonation of HMCs, respectively. Furthermore, when compared to the DTG plots of uncarbonated M-S and MS-S samples, a slight shift in the main decomposition peak from 405-425 to 434-438 °C was observed in the carbonated samples, which included the decomposition of carbonate phases. These decomposition patterns corresponded well with the temperature ranges stated in the literature [28, 30]. The decomposition temperatures and corresponding mass loss values revealed by the TG/DTG analysis were used to quantify the hydrate and carbonate phases within each sample, whose details are provided in Section 3.6.

3.6 Phase quantifications

Figures 8(a)-(d) show the deconvoluted DTG curves for all samples cured for 28 days. The original data (represented by the black dots) was included as well as the cumulative fit (represented by the solid line) for each sample, showing that a good fit was obtained in all cases. These two sets were accompanied with the deconvoluted curves, whose combination formed the cumulative fit. For each sample, the number

of deconvoluted curves varied, depending on the different types of hydrate and carbonate phases that decomposed during thermal analysis. For instance, for M-S sample, two main curves were used to represent the dehydration of adsorbed water (centered at ~128 °C) and dehydroxylation of brucite (centered at ~425 °C), along with the loss on ignition associated with impurities (e.g. undecomposed phases within MgO). In addition to these curves, two more curves (centered at ~263 and ~491 °C) were added to represent the mass loss associated with the decomposition of HMCs within M-C sample. Furthermore, the main curve (centered at ~430 °C) was deconvoluted into two curves that corresponded with the decompositions of brucite (centered at ~407 °C) and HMCs (centered at ~437 °C).

Differing from the M samples, MS samples included the decomposition of M-S-H in addition to other hydrate and carbonate phases. For MS-S sample, the three main phases referred to the dehydration of adsorbed water from M-S-H, dehydroxylation of brucite and dehydroxylation of M-S-H. While each of these 3 events was indicated by separate curves, the dehydration of M-S-H was represented by two individual curves referring to the water adsorbed on M-S-H surface and water confined in M-S-H pores [33]. For MS-C sample subjected to carbonation, 2 more curves were used to represent the dehydroxylation and decarbonation of HMCs (at ~224 and ~507 °C), in addition to the 3 decomposition reactions listed earlier for MS-S sample. Similar to M-C sample, the main curve (centered at ~434 °C) was divided into two to represent the decompositions of brucite and HMCs, in line with the findings of the previous literature on the thermal decomposition of HMCs [29, 34]. The area under each deconvoluted curve was calculated to find the mass loss corresponding to the relevant decomposition processes. During these calculations, the mass loss associated with the loss of ignition was also taken into account with respect to the binder component within each sample.

The mass loss values obtained from the deconvoluted DTG curves of all samples cured for 28 days are listed in Table 3. Similar to the phase formations shown by the XRD patterns in Figure 6, M-S sample revealed the formation of brucite as the main hydrate phase, which corresponded to ~20% of the total mass loss. The high brucite content within this sample was an indication of the lack of carbonation, whose progress was limited under the ambient CO_2 concentration used during the curing of

M-S. The introduction of carbonation in M-C sample led to the formation of HMCs (mass loss of ~14%), in addition to brucite (mass loss of ~5%). The smaller brucite content of M-C when compared to M-S revealed the progress of carbonation under the elevated (10%) CO_2 concentration used during the curing of M-C. Differing from sample M-S, a majority of brucite that formed as a result of the hydration reaction reacted with the CO_2 that diffused through the pore system, resulting in a notable formation of HMCs.

Similar to M samples, MS samples indicated different mass allocations with respect to their curing environments. MS-S sample indicated a high mass loss associated with the dehydroxylation of M-S-H (~6%), along with smaller amounts due to the dehydroxylation brucite (~3%). Out of all samples, MS-S revealed the highest mass loss due to adsorbed water, which was an indication of M-S-H formation. This was because dehydration of water absorbed on the surface of M-S-H as well as the water confined in M-S-H pores are known to contribute to the mass loss observed in this temperature range [33]. The use of carbonation in MS-C sample enabled a reduction of the amount of residual brucite (mass loss of ~0.5%), which almost disappeared at 28 days. This decline in the amount of brucite was related with its consumption in the formation of carbonate phases, along with M-S-H. Accordingly, the main mass loss observed in MS-C was linked with a significant formation of HMCs (mass loss of ~19%), accompanied with some M-S-H (mass loss of ~2%). The smaller amount of M-S-H formation within sample MS-C in comparison to MS-S, which corresponded well with the XRD patterns, could be associated with the utilization of Mg^{2+} in the carbonation reaction rather than its reaction with SiO_2 complexes to form M-S-H.

The reactions involving the formation of various hydrate and carbonate phases are dependent on several factors, one of them being the pH of the system, which can determine the dissolution of MgO and SiO_2, as well CO_2 into the pore solution. Therefore, the direction of the reactions that determine the M-S-H and HMC contents within carbonated MS systems are controlled by the concentration of the dissolved SiO_2 and CO_2, during which the dissolved element with the higher concentration preferentially reacts with Mg^{2+}. In this respect, the rate and degree of the reactions depend on the concentration of the dissolved element and the solubility product of M-S-H and HMCs. In this study, the overwhelming formation of HMCs when

compared to M-S-H in MS-C samples could be attributed to the higher dissolution of CO_2 gas (i.e. at a concentration of 10%) than that of solid SiO_2. Furthermore, the lower pH values induced with carbonation could have also enhanced the formation of HMCs [35, 36] rather than M-S-H, whose formation was shown to be favored at a higher pH of ≥ 10.5 [13, 37].

A comparison of the two carbonated samples, M-C and MS-C, revealed lower mass loss values corresponding to the formation of HMCs within the former (~14% vs. 19%). This difference in the amount of carbonate phases could be related to the variations in the type of carbonates, as well as the higher initial densities of M samples in comparison to MS samples, which could limit the amount of CO_2 diffusing through the sample pore network and thereby the overall amount of carbonates precipitating within the system. However, although M-C samples revealed a lower degree of carbonate formation, their higher densities enabled them to achieve generally higher strengths than MS-C samples during the earlier stages (≤ 28 days) of carbonation. The increased degree of carbonate formation within MS-C samples, coupled with the binding strength provided by M-S-H, led to almost equivalent strengths to those of M-C samples at 56 days (73 vs. 79 MPa). These results indicate that while sample density plays a key role in the reaction mechanisms and final performance, the progress of the carbonation reaction also contributes to strength development via the formation of an extensive carbonate network.

In addition to their physical properties, other factors such as the initial pH (i.e. controlled by the mix design and properties of the binder component), determine the extent of carbonation and hence the final performance of M and MS systems. The presence of SiO_2 has led to a lower initial pH of MS when compared to M samples, which may have provided a more favorable environment for HMC formation under carbonation [35, 36]. Furthermore, in purely MgO-based systems (M-C samples), the hydration and carbonation of MgO grains can lead to the formation of a solid hydrate/carbonate layer around the unreacted particles, thereby limiting further access to the unhydrated MgO particles. However, in MgO-SiO_2 systems (MS-C samples), since the dissolution of SiO_2 is lower than that of CO_2 under the given conditions, the presence of SiO_2 particles can provide nucleation seeding. This can enable the increased precipitation of $Mg(OH)_2$ available for carbonation, thereby

facilitating further carbonation and the associated formation of HMCs when compared to M samples.

4 Conclusions

This study investigated the performance and microstructural development of MgO and MgO-SiO_2 based concrete samples subjected to ambient and carbonation curing over a 56-day period. The density and strength results of the prepared samples were supported with a detailed microstructural study involving the use of XRD, TG/DTG and FESEM analyses. In addition to the evolution of sample microstructure, the data corresponding to the quantification of hydrate and carbonate phases within each formulation, obtained via thermal analysis, was used to explain the variations in sample performance.

MgO samples subjected to ambient curing revealed minimal strengths due to the inability of brucite to provide any binding strength between the cement paste and aggregates. A different scenario was observed in MgO-SiO_2 samples, which demonstrated a steady strength development due to the formation of M-S-H over the 56 days of curing. When compared to those cured under ambient conditions, the incorporation of carbonation curing led to an up to 412% and 57% increase in the strength of MgO and MgO-SiO_2 samples, respectively. Unlike the outcome of ambient curing, MgO samples subjected to CO_2 curing exhibited a rapid early strength development revealing strengths as high as 77 MPa at 7 days. This enhancement of performance was associated with the formation of carbonate phases in both MgO and MgO-SiO_2 samples, which led to the densification of sample microstructures. The formation of carbonates was accompanied with a reduction in the amount of hydrate phases in both formulations. The simultaneous formation of different carbonate phases such as nesquehonite, artinite, dypingite and hydromagnesite enabled the development of a dense and interconnected carbonate network within the carbonated samples.

The results of this study clearly demonstrated the critical role carbonation curing plays in the strength and microstructural development of MgO and MgO-SiO_2

formulations. A complete utilization of brucite, the intermediate hydrate phase, was observed in MgO-SiO_2 samples subjected to carbonation, which revealed an extensive formation of Mg-carbonates as well as M-S-H. Further studies on the optimization of the initial mix design and curing conditions can lead to even higher strengths by enabling the complete consumption of MgO in the hydration and subsequent carbonation reactions. This should be accompanied with an investigation of the effect of these parameters on the properties, stability and transformation of the final phases that form under different environments.

Acknowledgement

The authors would like to acknowledge the financial support from the Singapore MOE Academic Research Fund Tier 1 (RG 113/14) for the completion of this research project.

References

[1] J. Olivier, G. Janssens-Maenhout, M. Muntean, J. Peters, Trends in global CO2 emissions: 2015 Report. PBL Netherlands Environmental Assessment Agency, The Hague; European Commission, Joint Research Centre (JRC), Institute for Environment and Sustainability (IES), (2015).

[2] C. Unluer, A. Al-Tabbaa, Impact of hydrated magnesium carbonate additives on the carbonation of reactive MgO cements, Cement and Concrete Research, 54 (2013) 87-97.

[3] C. Unluer, A. Al-Tabbaa, Enhancing the carbonation of MgO cement porous blocks through improved curing conditions, Cement and Concrete Research, 59 (2014) 55-65.

[4] T. Zhang, L.J. Vandeperre, C.R. Cheeseman, Formation of magnesium silicate hydrate (MSH) cement pastes using sodium hexametaphosphate, Cement and Concrete Research, 65 (2014) 8-14.

[5] F. Jin, A. Al-Tabbaa, Thermogravimetric study on the hydration of reactive MgO and silica mixture at room temperature, Thermochimica Acta, 566 (2013) 162.

643 [6] W. Jiangxiong, C. Yimin, L. Yongxin, The reaction mechanism between MgO and
644 microsilica at room temperature, Journal of Wuhan University of Technology-
645 Materials Science Edition, 21 (2006) 88-91.
646 [7] T. Zhang, C. Cheeseman, L. Vandeperre, Development of low pH cement
647 systems forming magnesium silicate hydrate (MSH), Cement and Concrete
648 Research, 41 (2011) 439-442.
649 [8] T. Zhang, C. Cheeseman, L.J. Vandeperre, Characterisation of corrosion of
650 nuclear metal wastes encapsulated in magnesium silicate hydrate (MSH) cement,
651 Ceramic Materials for Energy Applications II, (2012) 159-167.
652 [9] T. Zhang, L.J. Vandeperre, C.R. Cheeseman, Magnesium-silicate-hydrate
653 cements for encapsulating problematic aluminium containing wastes, Journal of
654 Sustainable Cement-Based Materials, 1 (2012) 34-45.
655 [10] J. Szczerba, R. Prorok, E. Śnieżek, D. Madej, K. Maślona, Influence of time and
656 temperature on ageing and phases synthesis in the MgO–SiO2–H2O system,
657 Thermochimica Acta, 567 (2013) 57-64.
658 [11] F. Jin, A. Al-Tabbaa, Strength and hydration products of reactive MgO–silica
659 pastes, Cement and Concrete Composites, 52 (2014) 27-33.
660 [12] Y. Jia, B. Wang, Z. Wu, J. Han, T. Zhang, L.J. Vandeperre, C.R. Cheeseman,
661 Role of sodium hexametaphosphate in MgO/SiO2 cement pastes, Cement and
662 Concrete Research, 89 (2016) 63-71.
663 [13] Z. Li, T. Zhang, J. Hu, Y. Tang, Y. Niu, J. Wei, Q. Yu, Characterization of
664 reaction products and reaction process of MgO–SiO2–H2O system at room
665 temperature, Construction and Building Materials, (2014) 252-259.
666 [14] Z. Li, Q. Yu, X. Chen, H. Liu, J. Zhang, J. Zhang, Y. Yang, J. Wei, The role of
667 MgO in the thermal behavior of MgO–silica fume pastes, Journal of Thermal Analysis
668 and Calorimetry, 127 (2017) 1897-1909.
669 [15] N. Dung, C. Unluer, Improving the performance of reactive MgO cement-based
670 concrete mixes, Construction and Building Materials, 126 (2016) 747-758.
671 [16] L. Pu, C. Unluer, Investigation of carbonation depth and its influence on the
672 performance and microstructure of MgO cement and PC mixes, Construction and
673 Building Materials, 120 (2016) 349-363.
674 [17] M. Liska, A. Al-Tabbaa, Ultra-green construction: reactive magnesia masonry
675 products, Waste and Resource Management, 162 (2009) 185-196.

[18] M. Liska, A. Al-Tabbaa, Performance of magnesia cements in pressed masonry units with natural aggregates: Production parameters optimisation, Construction and Building Materials, 22 (2008) 1789-1797.
[19] M. Liska, A. Al-Tabbaa, K. Carter, J. Fifield, Scaled-up commercial production of reactive magnesia cement pressed masonry units. Part II: Performance, Construction Materials, 165 (2012) 225-243.
[20] M. Liska, L. Vandeperre, A. Al-Tabbaa, Influence of carbonation on the properties of reactive magnesia cement-based pressed masonry units, Advances in cement research, 20 (2008) 53-64.
[21] N. Dung, C. Unluer, Sequestration of CO2 in reactive MgO cement-based mixes with enhanced hydration mechanisms, Construction and Building Materials, 143 (2017) 71-82.
[22] S. Ruan, C. Unluer, Effect of air entrainment on the performance of reactive MgO and PC mixes, Construction and Building Materials, 142 (2017) 221-232.
[23] N. Dung, C. Unluer, Carbonated MgO concrete with improved performance: The influence of temperature and hydration agent on hydration, carbonation and strength gain, Cement and Concrete Composites, 82 (2017) 152-164.
[24] L.J. Vandeperre, A. Al-Tabbaa, Accelerated carbonation of reactive MgO cements, Advances in Cement Research, 19 (2007) 67-79.
[25] Y. Gao, H. Wang, Y. Su, Q. Shen, D. Wang, Influence of magnesium source on the crystallization behaviors of magnesium hydroxide, Journal of Crystal Growth, 310 (2008) 3771-3778.
[26] J. Chen, T. Li, X. Li, K.C. Chou, X. Hou, Some new perspective on the reaction mechanism of MgO–SiO2–H2O system, International Journal of Applied Ceramic Technology, 13 (2016) 1164-1172.
[27] D. Bhattacharjya, T. Selvamani, I. Mukhopadhyay, Thermal decomposition of hydromagnesite, Journal of Thermal Analysis and Calorimetry, 107 (2012) 439-445.
[28] J. Lanas, J.I. Alvarez, Dolomitic lime: thermal decomposition of nesquehonite, Thermochimica Acta, 421 (2004) 123-132.
[29] L.A. Hollingbery, T.R. Hull, The thermal decomposition of huntite and hydromagnesite—A review, Thermochimica Acta, 509 (2010) 1-11.
[30] V. Vágvölgyi, R.L. Frost, M. Hales, A. Locke, J. Kristóf, E. Horváth, Controlled rate thermal analysis of hydromagnesite, Journal of Thermal Analysis and Calorimetry, 92 (2008) 893-897.

[31] B. Lothenbach, D. Nied, E. L'Hôpital, G. Achiedo, A. Dauzères, Magnesium and calcium silicate hydrates, Cement and Concrete Research, 77 (2015) 60-68.
[32] D. Nied, K. Enemark-Rasmussen, E. L'Hopital, J. Skibsted, B. Lothenbach, Properties of magnesium silicate hydrates (MSH), Cement and Concrete Research, 79 (2016) 323-332.
[33] M. Tonelli, F. Martini, L. Calucci, E. Fratini, M. Geppi, F. Ridi, S. Borsacchi, P. Baglioni, Structural characterization of magnesium silicate hydrate: towards the design of eco-sustainable cements, Dalton Transactions, 45 (2016) 3294-3304.
[34] G. Jauffret, J. Morrison, F. Glasser, On the thermal decomposition of nesquehonite, Journal of Thermal Analysis and Calorimetry, 122 (2015) 601-609.
[35] P. Ballirano, C. De Vito, S. Mignardi, V. Ferrini, Phase transitions in the Mg CO 2 H 2 O system and the thermal decomposition of dypingite, Mg 5 (CO 3) 4 (OH) 2· 5H 2 O: Implications for geosequestration of carbon dioxide, Chemical Geology, 340 (2013) 59-67.
[36] V. Ferrini, C. De Vito, S. Mignardi, Synthesis of nesquehonite by reaction of gaseous CO2 with Mg chloride solution: its potential role in the sequestration of carbon dioxide, Journal of Hazardous Materials, 168 (2009) 832-837.
[37] M. Tonelli, F. Martini, L. Calucci, M. Geppi, S. Borsacchi, F. Ridi, Traditional Portland cement and MgO-based cement: a promising combination?, Physics and Chemistry of the Earth, Parts A/B/C, (2017).

List of Tables:

Table 1 Chemical composition and physical properties of MgO and microsilica (provided by suppliers).

	MgO	Microsilica
Chemical composition		
MgO	>91.5%	-
CaO	1.6%	-
SiO_2	2.0%	>90%
Al_2O_3	<0.7%	-
LOI	4%	<3%
Physical properties		
Particle size (%)	<74 µm 95% min	>45 µm 1.5% max
Bulk density (kg/dm^3)	-	0.20-0.35

Table 2 Mix compositions and corresponding curing conditions.

Sample	Composition (wt.%)			Curing condition
	MgO	Microsilica	Coarse aggregates	
M-S	40	0	60	Sealed
M-C	40	0	60	Carbonated
MS-S	20	20	60	Sealed
MS-C	20	20	60	Carbonated

Table 3 Allocation of mass loss revealed during the thermal decomposition of samples cured for 28 days, based on the deconvoluted DTG curves.

Sample	Mass loss (% of original mass)			
	Adsorbed water (dehydration)	Brucite (dehydroxylation)	M-S-H (dehydroxylation)	HMCs (dehydroxylation/ decarbonation)
M-S	2.2	19.9	-	-
M-C	2.4	5.1	-	14.2
MS-S	7.3	2.8	6.4	-
MS-C	4.2	0.5	2.2	19.0

List of Figures:

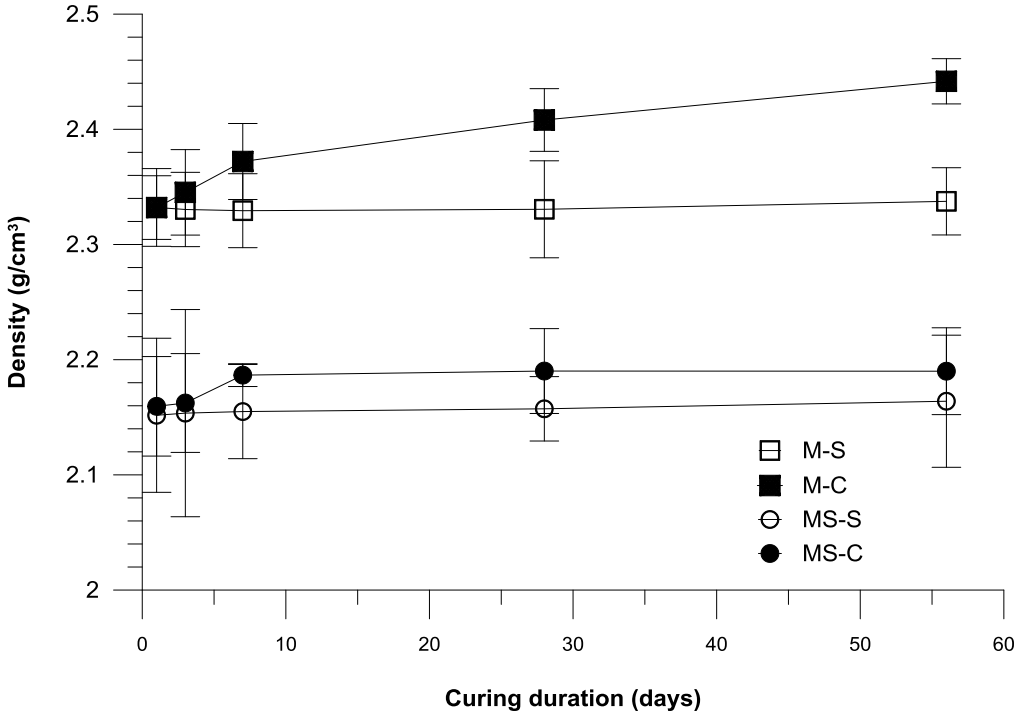

Figure 1 Density of all samples during 56 days of curing

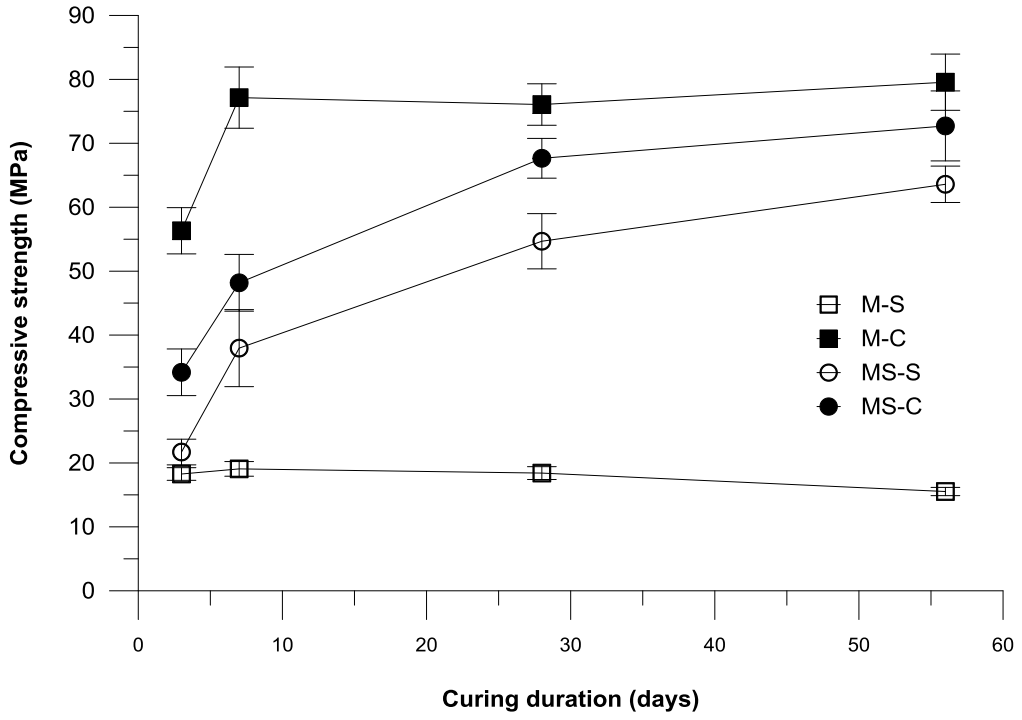

Figure 2 Compressive strength of all samples subjected to 56 days of curing

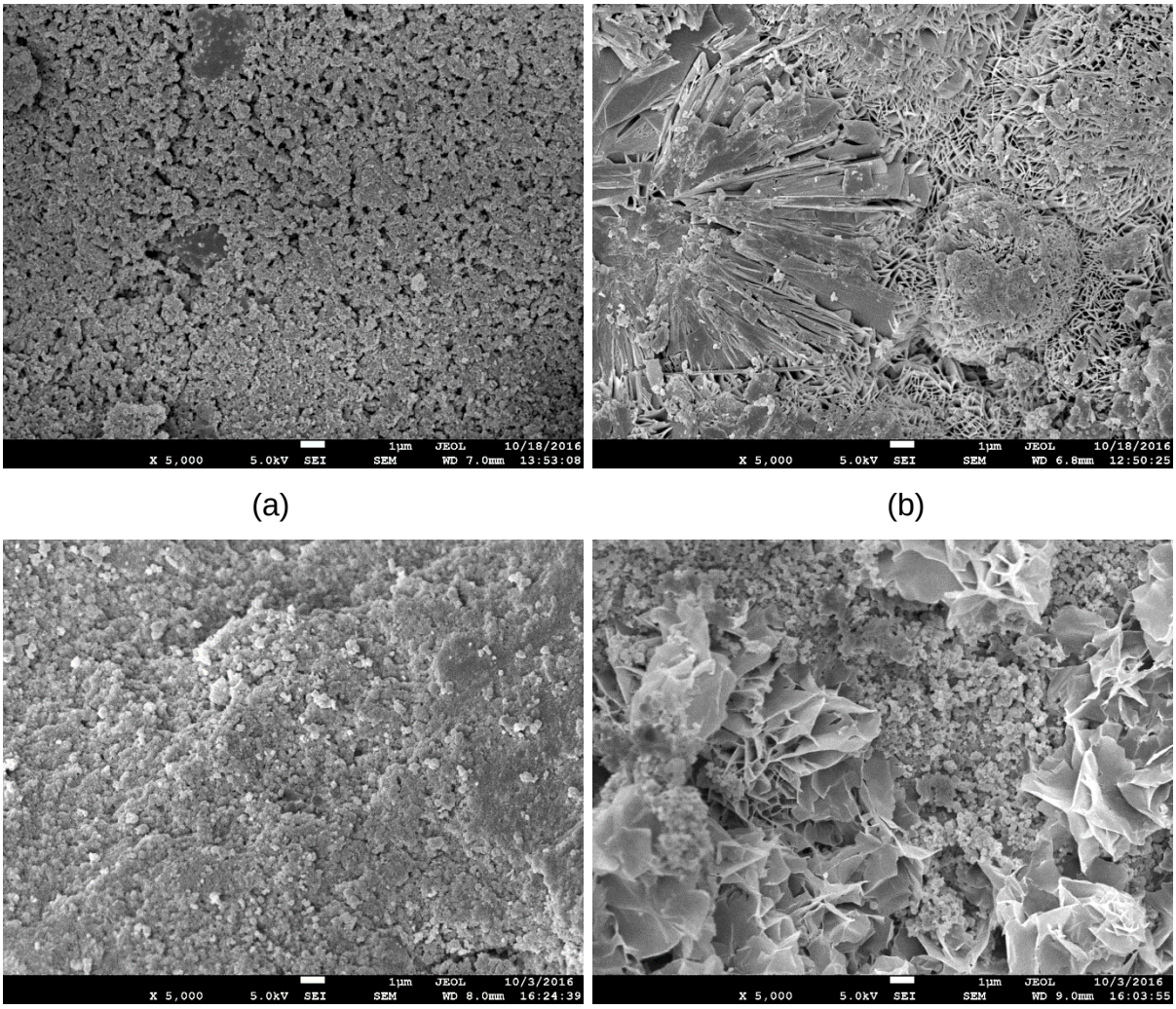

(a) (b)

(c) (d)

Figure 3 FESEM images of (a) M-S, (b) M-C, (c) MS-S and (d) MS-C samples at 3 days

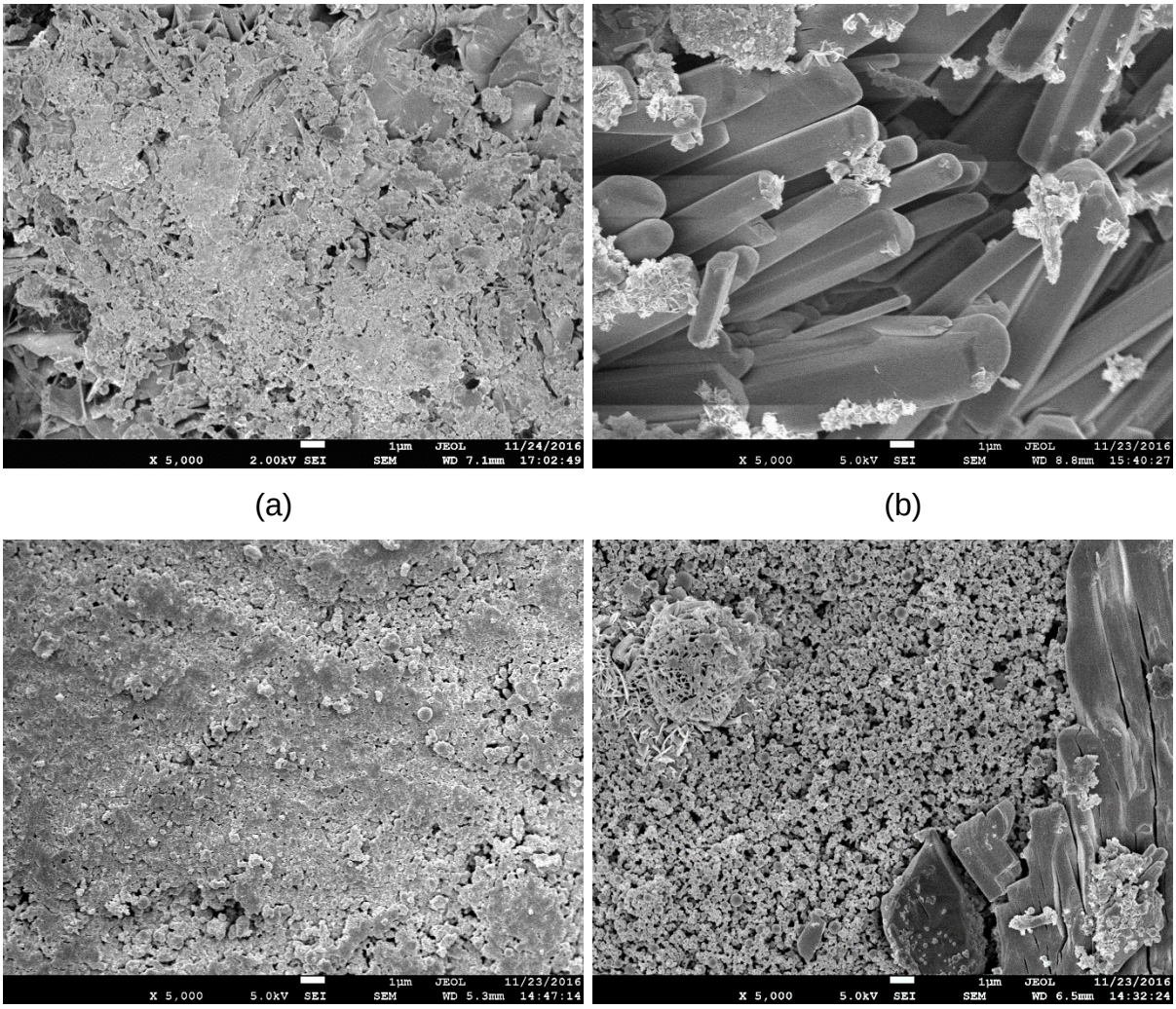

Figure 4 FESEM images of (a) M-S, (b) M-C, (c) MS-S and (d) MS-C samples at 28 days

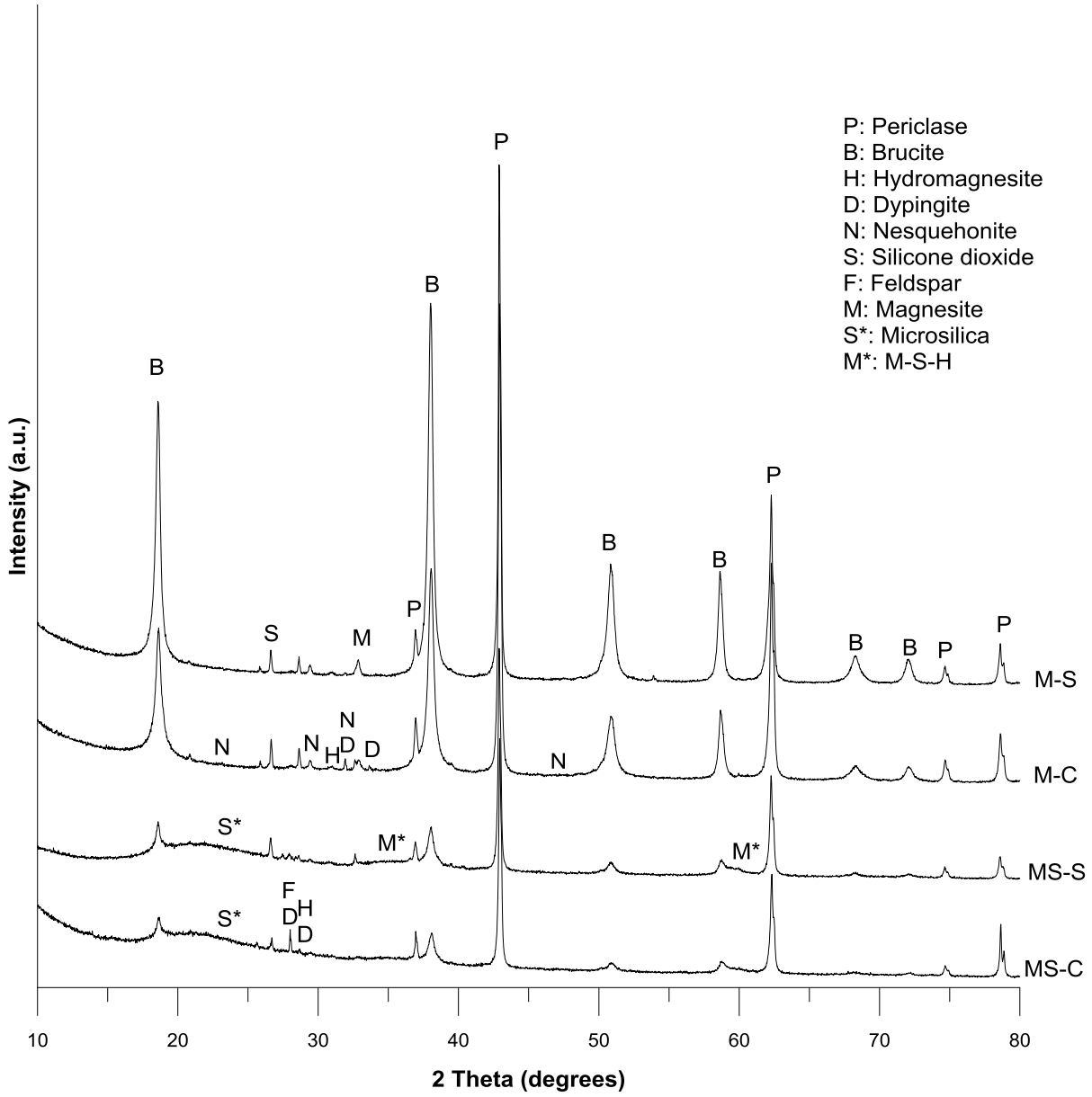

Figure 5 XRD diffractograms of all samples at 3 days

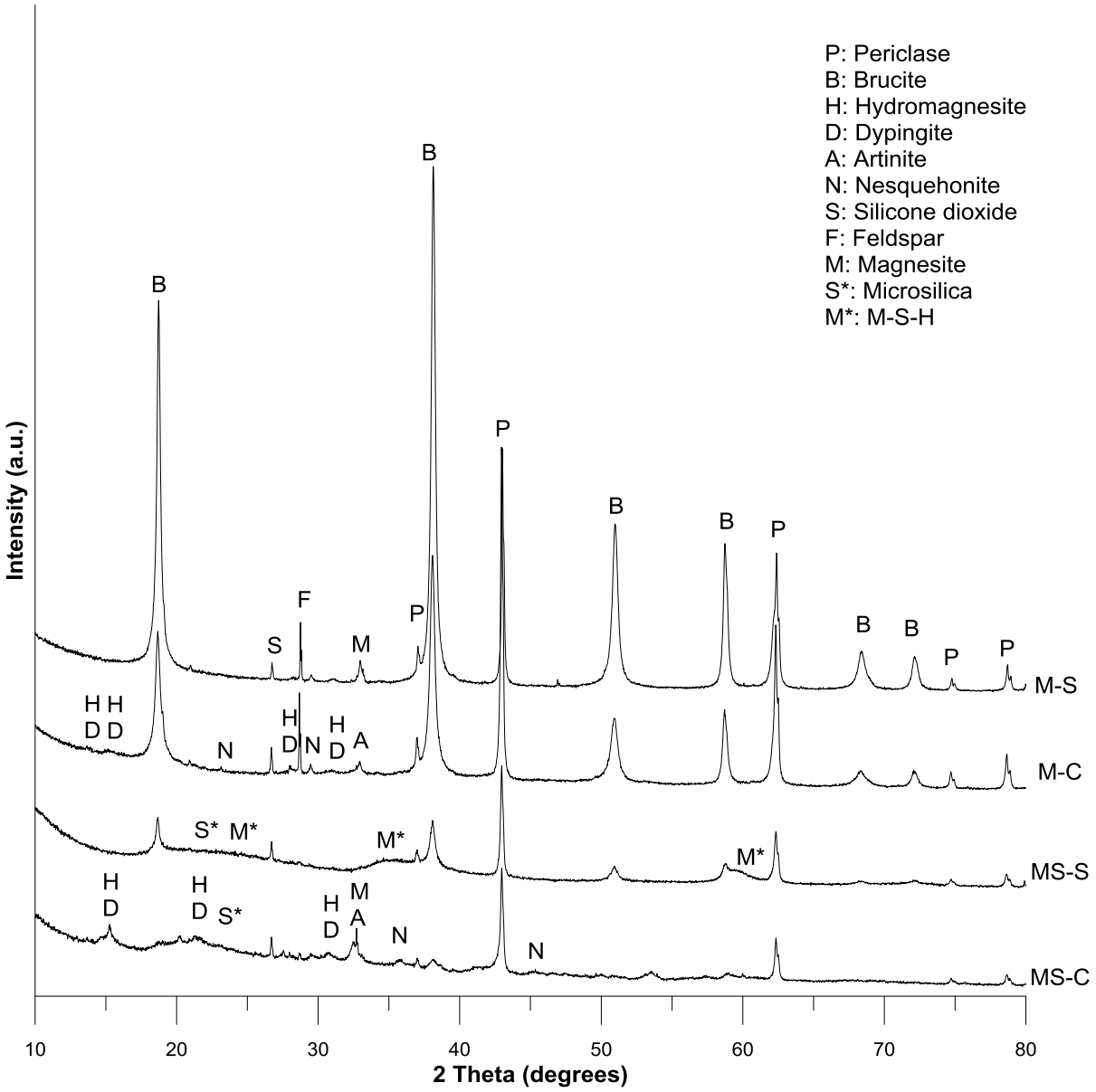

Figure 6 XRD diffractograms of all samples at 28 days

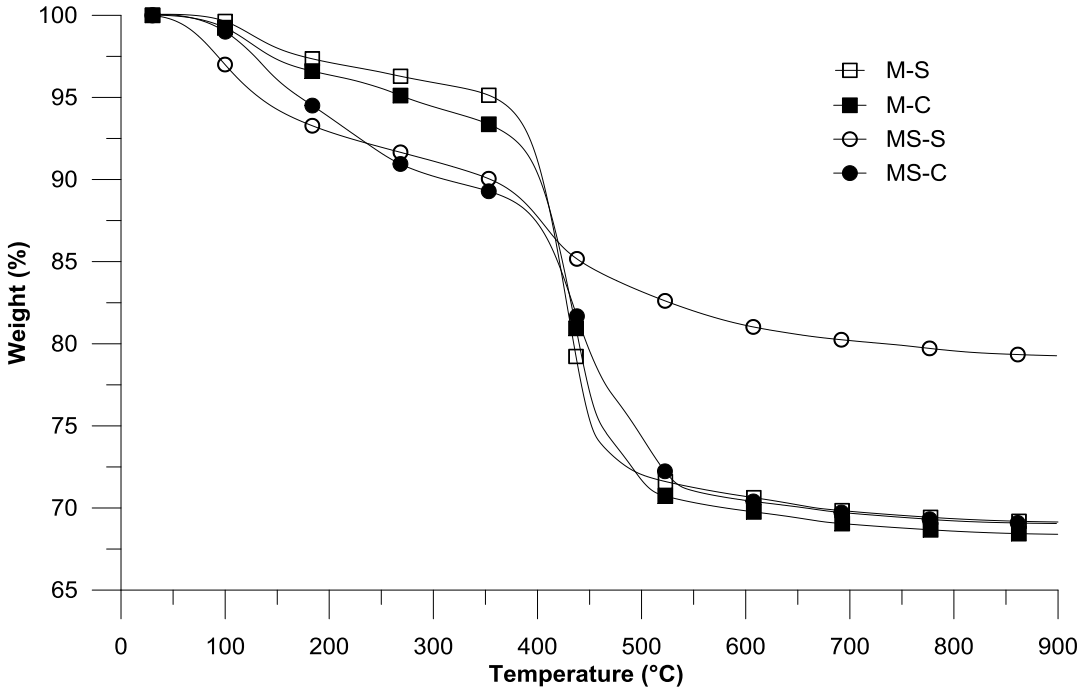

(a)

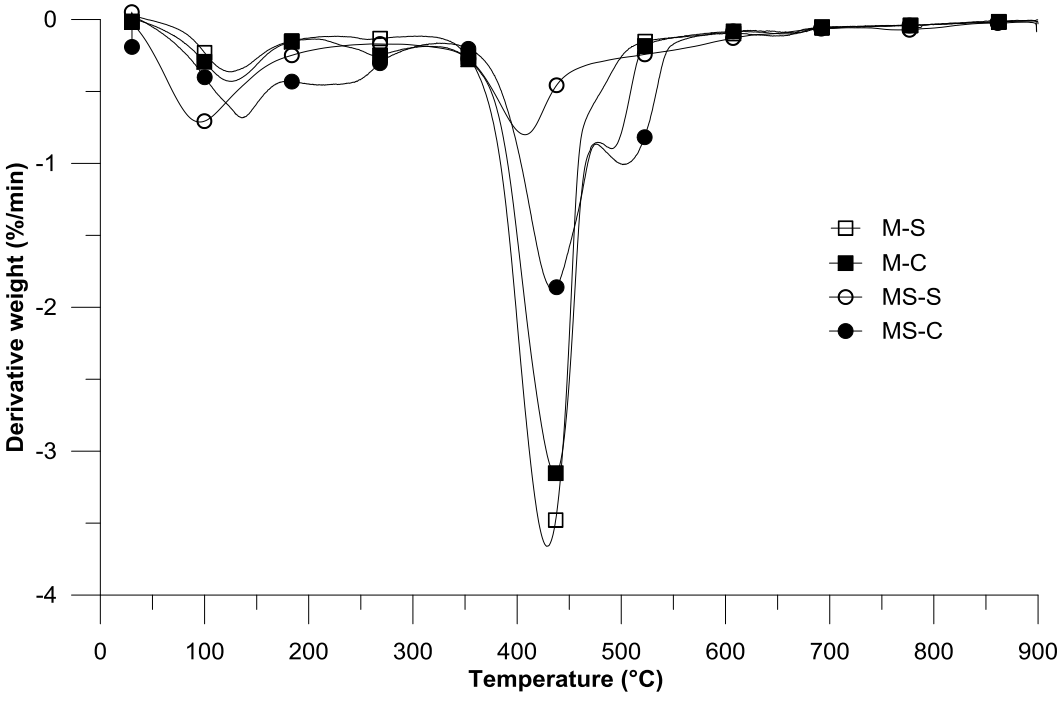

(b)

Figure 7 Thermogravimetric analysis results of all samples at 28 days, showing the (a) TG and (b) DTG plots

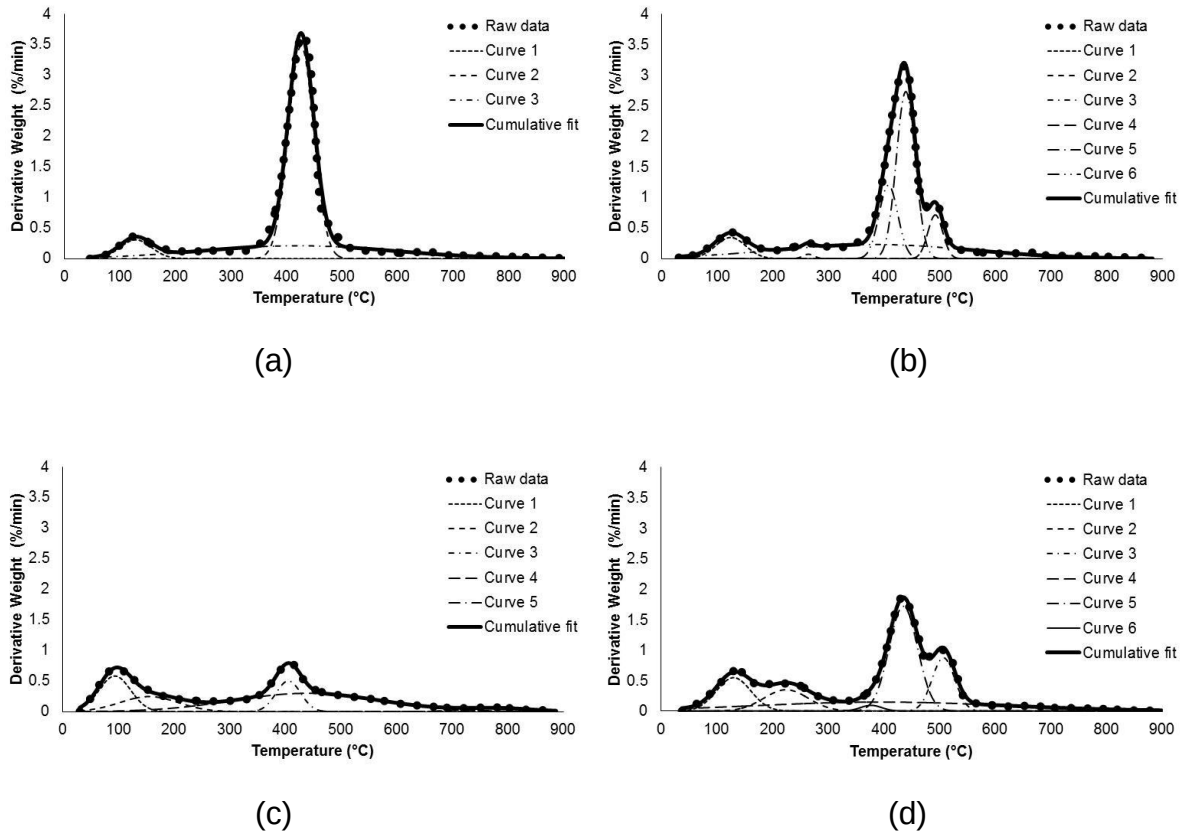

Figure 8 Deconvolution of DTG curves of (a) M-S, (b) M-C, (c) MS-S and (d) MS-C samples at 28 days